Geochemistry Geophysics Geosystems G3
AN ELECTRONIC JOURNAL OF THE EARTH SCIENCES
Published by AGU and the Geochemical Society

Technical Brief
Volume 9, Number 7
17 July 2008
Q07014, doi:10.1029/2008GC002032
ISSN: 1525-2027

Click Here for Full Article

Prediction of anisotropy from flow models: A comparison of three methods

Einat Lev and Bradford H. Hager

Department of Earth, Atmospheric and Planetary Science, Massachusetts Institute of Technology, 77 Massachusetts Avenue, Cambridge, Massachusetts 02139, USA (einatlev@mit.edu)

[1] Observations of anisotropy in Earth are used regularly as constraints for models of deformation, using various assumptions about the relationship between deformation and the resulting anisotropic fabric. We compare three methods for calculating fabric from velocity fields: tracking of finite strain ellipses, a kinematic crystallographic code, and the evolution of directors. We find that the use of the finite strain ellipse provides only limited prediction capabilities, as it cannot reproduce experimental observations that involve recrystallization. The crystallographic code we tested (a variant of the popular code D-Rex) provides a more complete fabric prediction, but at a much higher computational cost. The directors method provides an intermediate solution: while it does not include some of the more complex crystallographic processes that D-Rex does, the results of this method closely resemble those of D-Rex, at a lower computational cost. The directors are also capable of tracking anisotropy at much larger strains than D-Rex. We conclude that when computation speed is important, for example, in self-consistent geodynamic models with anisotropic rheology, the directors method provides an appropriate approximation.

Components: 6913 words, 11 figures.

Keywords: anisotropy; flow models; mantle dynamics.

Index Terms: 1213 Geodesy and Gravity: Earth's interior: dynamics (1507, 7207, 7208, 8115, 8120); 1236 Geodesy and Gravity: Rheology of the lithosphere and mantle (7218, 8160); 8194 Tectonophysics: Instruments and techniques.

Received 15 March 2008; **Revised** 7 May 2008; **Accepted** 16 May 2008; **Published** 17 July 2008.

Lev, E., and B. H. Hager (2008), Prediction of anisotropy from flow models: A comparison of three methods, *Geochem. Geophys. Geosyst.*, *9*, Q07014, doi:10.1029/2008GC002032.

1. Introduction

[2] Understanding the way in which the lithosphere and the mantle deform is among the most fundamental goals of geodynamics. In recent years, observations of seismic anisotropy have been used extensively in attempts to constrain the deformation in Earth's interior at a wide range of tectonic settings and depths [e.g., *Fischer and Wiens*, 1996; *Maupin et al.*, 2005; *Fouch and Rondenay*, 2006]. The basic assumption made in this field of research is that deformation of geologic material results in the development of lattice preferred orientation (LPO), leading, in turn, to anisotropy of observables such as seismic wave speed and electrical conductivity.

[3] The above assumption is supported by many natural examples of mantle rocks that exhibit strong textures [*Ben-Ismail et al.*, 2001; *Mehl et al.*, 2003], by laboratory experiments [*Zhang and Karato*, 1995; *Jung and Karato*, 2001] and by theoretical calculations [*Kaminski and Ribe*,

Copyright 2008 by the American Geophysical Union

2001; *Tommasi et al.*, 2000; *Blackman et al.*, 2002] which exemplify the relationships between applied deformation and the development of preferred orientation. Usually these studies find an alignment of the LPO with the direction of shearing or extension, and this is commonly the form of anisotropy interpreted from flow models. However, both natural and laboratory samples display complexity, with dependence on volatile content, degree of melting, pressure and stress conditions [*Jousselin and Mainprice*, 1998; *Jung and Karato*, 2001].

[4] Thanks to the increasing availability of measurements of seismic and conductive anisotropy in many regions of the Earth [e.g., *Montagner*, 1998; *Savage*, 1999; *Weiss et al.*, 1999; *Simpson*, 2002; *Baba et al.*, 2006], it is becoming feasible to use them to constrain geodynamic models. Specifically, it may be possible to use anisotropy to distinguish between competing models based on the differences in the predicted anisotropy. It is thus clear that an accurate technique for predicting anisotropy from a given geodynamic model is valuable, and that the differences between various prediction methods need to be identified. Additionally, it is important to track the anisotropy that develops during mantle flow as it can influence the deformation [*Lev and Hager*, 2008]. Mantle materials are often mechanically anisotropic [e.g., *Durham and Goetze*, 1977; *Pouilloux et al.*, 2007], and knowing the texture is essential for modeling the flow accurately.

[5] In this paper, we discuss three methods for predicting anisotropy from geodynamical flow models: the use of finite strain ellipses, a kinematic crystallographic method (following *Kaminski et al.* [2004]), and tracking a set of directors [*Mühlhaus et al.*, 2004]. We begin by describing the details of each method and then compare the fabrics that the three methods predict for several flows of increasing complexity. We then consider the computational cost of the methods, a factor that strongly affects their usefulness for integration with large-scale flow models.

2. Methods

[6] In recent years, many studies have attempted to predict the anisotropic fabric that develops during deformation in the mantle. Two of the more popular techniques are the tracking of finite strain [e.g., *McKenzie*, 1979; *Ribe*, 1992; *Hall et al.*, 2000; *Becker et al.*, 2003; *Long et al.*, 2007] and the employment of the kinematic crystallographic code D-Rex [*Kaminski et al.*, 2004], for example, by *Becker et al.* [2006a, 2006b] and *Marquart et al.* [2007]. A third method we discuss here, the tracking of directors, was adopted from the field of liquid crystal physics for the purpose of including anisotropic viscosity in geodynamic flow models [*Moresi et al.*, 2003]. An additional method for predicting anisotropic fabric from flow models, which is not considered in this paper, is the polycrystal plasticity method (VPSC) [e.g., *Wenk et al.*, 2006]. VPSC is computationally intensive and thus it is not as readily available for straightforward incorporation into flow models and is not discussed in this paper. The application of VPSC for predicting mantle anisotropy is discussed by *Tommasi et al.* [2000], who performed a detailed comparison between VPSC and an equilibrium-based model [*Chastel et al.*, 1993], as well as by *Blackman et al.* [2002].

[7] The common input to all three methods we discuss here is a velocity field, calculated analytically or numerically, through which tracer particles (“aggregates”) are propagated. The anisotropy is calculated in steps along the path, in the manners described below.

2.1. Tracking of the Finite Strain Ellipse

[8] The tracking of the long axis of the finite strain ellipse (FSE) is a commonly used technique for predicting seismic anisotropy from flow models [*Hall et al.*, 2000; *Becker et al.*, 2003; *Long et al.*, 2007]. In these studies, the orientation of the major axis of the FSE is assumed to represent the orientation of the olivine *a* axis and the direction of fast wave propagation. The stretched length of the FSE is taken as a proxy for the percentage of anisotropy.

[9] In the calculation of the finite strain ellipse, we follow the formulation of *McKenzie* [1979], solving the following time evolution equation:

$$\dot{F} = LF \tag{1}$$

where F is the finite strain tensor, $\dot{F}$ is its time derivative, L is the velocity gradient tensor, and the finite strain tensor at time $t = 0$ is the identity matrix I.

[10] For simple cases, such as simple or pure shear, equation (1) can be solved analytically. For more complicated cases, this equation can be solved numerically using methods such as a time-centered scheme [*McKenzie*, 1979] or a fourth-order Runge-Kutta scheme.

[11] For each step, we calculate the direction of the major axis of the finite strain ellipse and its magnitude using the inverse Cauchy strain tensor, C [*Malvern*, 1969]:

$$C = \left(F^{-1}\right)^T F^{-1} \quad (2)$$

The major axis of the strain ellipse is oriented in the direction of the eigenvector associated with the largest eigenvalue of C.

2.2. FedRex, the Forward Evolution D-Rex

[12] D-Rex [*Kaminski et al.*, 2004] is a popular program for calculating seismic anisotropy resulting from the development of crystal lattice preferred orientation in response to a velocity field. It enables tracking of olivine and enstatite aggregates through a flow field and supports texture evolution through plastic deformation and dynamic recrystallization by grain rotation and sliding. The equations controlling the time evolution of the texture are described by *Kaminski and Ribe* [2001, 2002], as well as *Browaeys and Chevrot* [2004]. D-Rex was used recently in combination with flow models to predict global [*Becker et al.*, 2006a] and regional [*Becker et al.*, 2006b] seismic anisotropy. Because most observations of seismic anisotropy are interpreted in terms of hexagonal symmetry and the orientation of the olivine a axis, the output of D-Rex we use here is the fast orientation resulting from reducing the full elastic tensor to its hexagonal symmetry projection.

[13] For our purpose here we implemented a modification of D-Rex, named FedRex. In our modified code, particles are advected only forward in time, which makes the code faster than the publicly available version. The input velocity field to FedRex may change over time. Additionally, each particle may have a unique composition and crystallographic properties. In the future, our code can be easily extended to include the effects of local variations in temperature, pressure and volatile content. As part of the development of FedRex, we made it fully three-dimensional, and added new features such as calculating the percentage of LPO contributed by various symmetries and output of the grain Euler angles. FedRex uses the same crystallographic input parameters used in D-Rex: grain boundary mobility (M) and grain boundary sliding threshold (χ).

[14] One unique feature of D-Rex compared with other crystallographic codes and with the FSE method is the consideration of recrystallization. Recrystallization causes LPO to adjust faster to a shear direction than the FSE axis. The implications of this difference were demonstrated previously by *Marquart et al.* [2007], who compared the predictions from the two methods for a model of a plume interacting with a mid-ocean ridge. They found significant deviations between the LPO predicted by FSE and by D-Rex. After comparing the predictions with observations of seismic anisotropy for Iceland they concluded that the calculations using D-Rex agree with the data better than the FSE calculation.

2.3. Directors Evolution

[15] The "directors," a term adopted from material sciences and the study of liquid crystals, can be thought of as normal vectors to the planes of easy glide. The use of directors implicitly assumes a cubic or hexagonal symmetry. The directors define the axis of symmetry of the crystal, aggregate or parcel, which can then be used to determine the rotation of the elasticity or viscosity tensor. The relationship between the director and planes of easy glide in olivine in the context of mantle flow is depicted in Figure 1.

[16] The directors are advected in space similarly to particles. The orientation of each director, denoted by the vector **n**, evolves in response to velocity gradients in the surroundings of the director:

$$\dot{n}_j = -L_{i,j} n_i \quad (3)$$

where i, j relate to the coordinates and $L_{i,j}$ is the (i, j) component of the velocity gradient tensor [*Mühlhaus et al.*, 2004]. The average orientation at a grid element is then calculated using averaging of the director orientations. To compare with the predictions of fast orientations resulting from FSE and FedRex, we assume here that the fast axis of each particle is perpendicular to the director. The strength of the anisotropy is calculated using the M index [*Skemer et al.*, 2005], an estimate of the mutual misorientation of the particles with each other. Section 4.3 describes in more detail the mapping between directors and seismic anisotropy, including the particular case of olivine.

[17] In rocks, the process of dynamic recrystallization leads to rapid alignment of crystals with the direction of shear [*Karato*, 1988]. To mimic this process, we added a forced realignment of the directors. We track the accumulated stretching of each director, and after a prescribed threshold (denoted here by ξ) is reached, we realign the

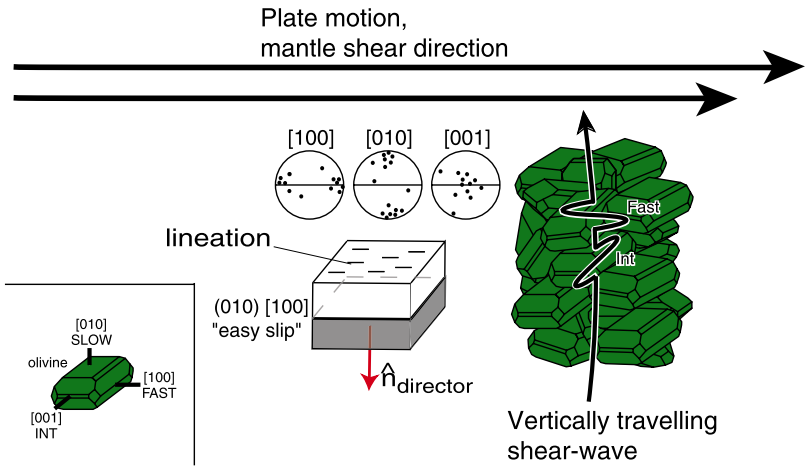

Figure 1. The relationship between directors, olivine LPO, and seismic anisotropy. We show here olivine LPO type A, in which the dominant slip system is (010)[100]. The director is thus parallel to the b axis, and the lineation, deduced from the local shear direction, parallels the a axis. This algorithm allows for a rapid prediction of seismic anisotropy, represented here by the splitting of a vertically traveling shear wave (e.g., SKS). The schematic pole figures illustrate the distribution of crystal orientations in the aggregate shown. The inset in the bottom left corner identifies the relative seismic wave speeds in association with olivine crystal axes. The original version of this figure was prepared by L. Mehl and J. Warren.

director to be normal to the local infinite strain axis (ISA). We calculate the ISA similarly to *Kaminski and Ribe* [2002, Appendix A], by taking the longest eigenvector of the matrix $U = F^T F = \exp(L\tau_\infty)^T \exp(L\tau_\infty)$ of the local velocity. In purely rotational parts of the flow, where the ISA is not defined, we use the orientation calculated by equation (3). In the future, the realignment threshold, ξ, may be made sensitive to temperature, composition and other local conditions. The use of a discrete threshold and realignment to simulate the continuous process of recrystallization is valid when a large enough set of directors is being tracked together and averaged over. We find that in the flows examined here, a set of 40 directors per aggregate or finite element was sufficient to give a smooth transition between a randomly oriented set to a fully aligned set.

[18] We use the tests described below to calibrate the stretching threshold. After this realignment, the director is not stretched any further. Since the directors methods tracks a group of directors which orientations are then averaged to obtain the orientation of the aggregate, this realignment with the shear direction is gradual and smooth, similarly to recrystallization in natural rocks. Applying a similar realignment on an individual director or finite strain ellipse would lead to a sharp and unnatural transition.

[19] One advantage of the directors method over crystallographic methods such as FedRex and VPSC is its ability to track very large strains. This makes the directors method more applicable for integration with mantle flow models, especially such that span long time periods.

3. Tests and Results

[20] We compare the resulting fabric predicted by the three methods in three tests with increasing levels of complexity. Figure 2 illustrates schematically the test setups. We first calibrate the free parameters for each method using a two-dimensional (2-D) plane strain simple shear model. We continue with another steady state model, of a 1 × 1 convection cell, starting with initially isotropic material throughout the model domain and then examining the fabric at specified time intervals. Last, we look at a case of 2-D time-dependent flow resulting from an instability of a dense material sinking into a more buoyant substratum (Figure 2c). The velocity field for this test was generated using the finite element code Underworld [*Moresi et al.*, 2003] assuming an isotropic, Newtonian rheology.

3.1. Simple Shear

[21] The results of the simple shear tests are presented in Figure 3. We plot the orientation of the major axis of the finite strain ellipse (cyan) and

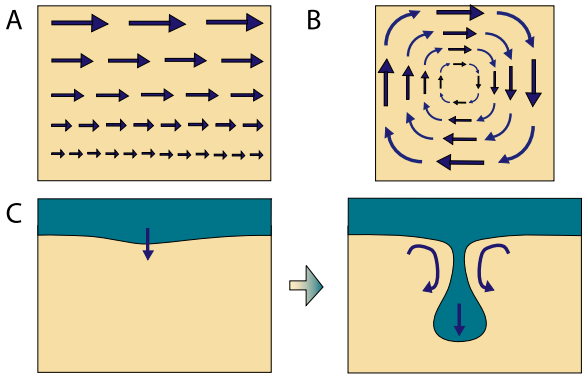

Figure 2. Schematic diagrams showing the flow fields in the three tests addressed in this paper. (a) Simple shear, used for validation of the calculations and for calibration of parameters; (b) 1 × 1 convection cell; (c) Rayleigh-Taylor instability, a sinking dense "drip."

that of the average olivine *a* axis (red is FedRex, blue and gray shades are directors) with respect to the direction of shearing (horizontal). For comparison, we also show the results of the laboratory experiments on olivine by *Zhang et al.* [2000]. The input parameters to FedRex (M = 125, λ = 5, χ = 0.3) are those found by *Kaminski et al.* [2004] to best fit experimental results.

[22] We find, not surprisingly, that when no forced realignment occurs ($\xi = \infty$), the average of director A axes follows the finite strain ellipse. The directors closely agree with the results of FedRex and the lab experiments when the stretching threshold is set to approximately 1.5. *Kaminski and Ribe* [2001] find that a grain boundary sliding threshold of (grain size/initial grain size) = χ = 0.3 gives a good fit to experiments. We tested FedRex under simple shear conditions and found that this value of χ is reached after a stretching of 60% (natural strain = 0.47). This value compares well with the stretching threshold of ξ = 1.5 we find for the directors.

3.2. Steady State 1 × 1 "Convection Cell"

[23] The input velocity field used here is defined as

$$V_x = \cos\left(\frac{\pi x}{2}\right)\sin\left(\frac{\pi z}{2}\right)$$
$$V_z = -\sin\left(\frac{\pi x}{2}\right)\cos\left(\frac{\pi z}{2}\right) \quad (4)$$

where x, z are the coordinates, both ranging from −1 to +1. Note that for this velocity field, the off-diagonal components of the velocity gradient tensor encountered by the particle along its path stay almost constant, while the diagonal components, associated with pure shear, change.

[24] In Figure 4 we show the velocity field used in this test (red arrows), and the resulting fabric for one particle tracked along a complete round trip path. Yellow bars show the *a* axis calculated by FedRex scaled by the percent of anisotropy (ranging from 1 to 14%). Black ellipses show the finite strain ellipses, and rose diagrams show the distri-

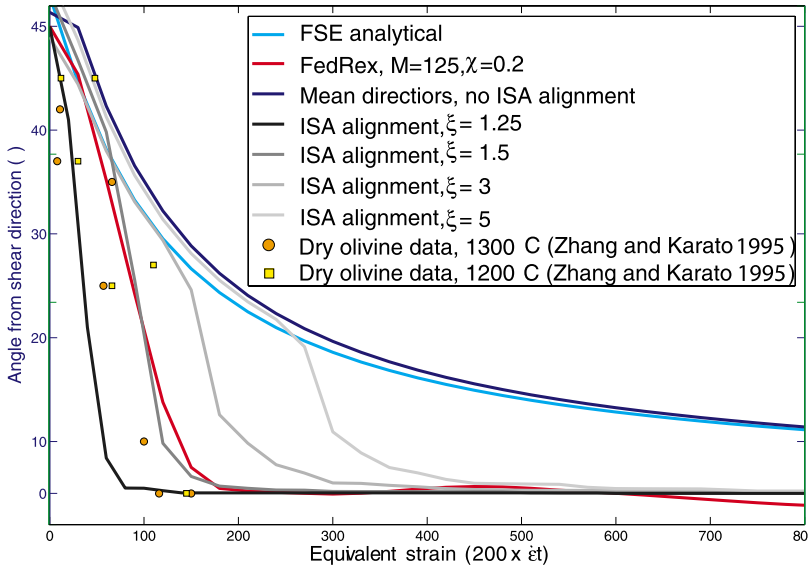

Figure 3. Results of the simple shear test. Plotted are the inclination of the finite strain ellipse and the A axis of olivine calculated using the three methods. For FedRex, M is the grain boundary mobility, and χ is the grain boundary sliding threshold. For the directors method with infinite strain axis (ISA) alignment, ξ is the stretching threshold for realignment. Also shown are laboratory experiment results from *Zhang and Karato* [1995].

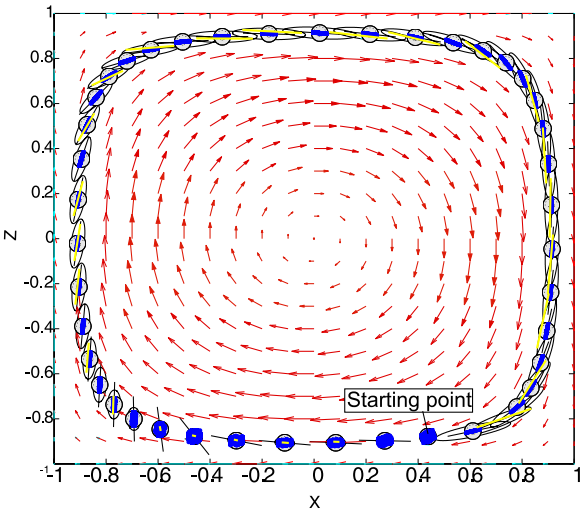

Figure 4. Results of a convection cell test. At each step we plot the finite strain ellipse (black ellipses) and its major axis, the A axis orientation calculated by FedRex (yellow lines), and the distribution of A axes using a set of directors (blue rose diagrams). Clearly, all methods agree with each other soon after the beginning of the path.

bution of director A axis orientations. It is clear that the fabrics from all three methods agree after the particle has turned the first corner and any original fabric is annealed. However, in a more variable flow field, differences could arise.

3.3. Time-Dependent Layered-Density Instability

[25] Many geodynamic studies predicting anisotropy assume steady state flow. However, flow fields in the mantle are often not in steady state: plate geometry evolves with time, subduction initiates and ceases, continents collide and break apart and plumes and drips grow off unstable boundary layers. It is thus important to consider the effects of time-dependent flow fields on the evolving anisotropy. We examine this effect using a simple model of a "drip," a Rayleigh-Taylor instability driven by the negative buoyancy of an overlaying layer. This process is intrinsically unstable and is not at steady state until a complete density overturn is reached. In Figure 5 we plot the paths of particles starting at the same point and advected by each of the varying velocity fields assuming that each field is kept constant; the paths are clearly different. We also plot the "real" path of a particle starting at this point and advected by the changing velocity field. This path is different from all the steady state paths.

[26] In this test, we analyze both the evolution of a single particle, and the evolution of the whole model domain, which we initialize as having no LPO. The input parameters for FedRex are those preferred by *Kaminski and Ribe* [2001] and the stretching threshold for the Directors is $\xi = 1.5$, following the results of section 3.1.

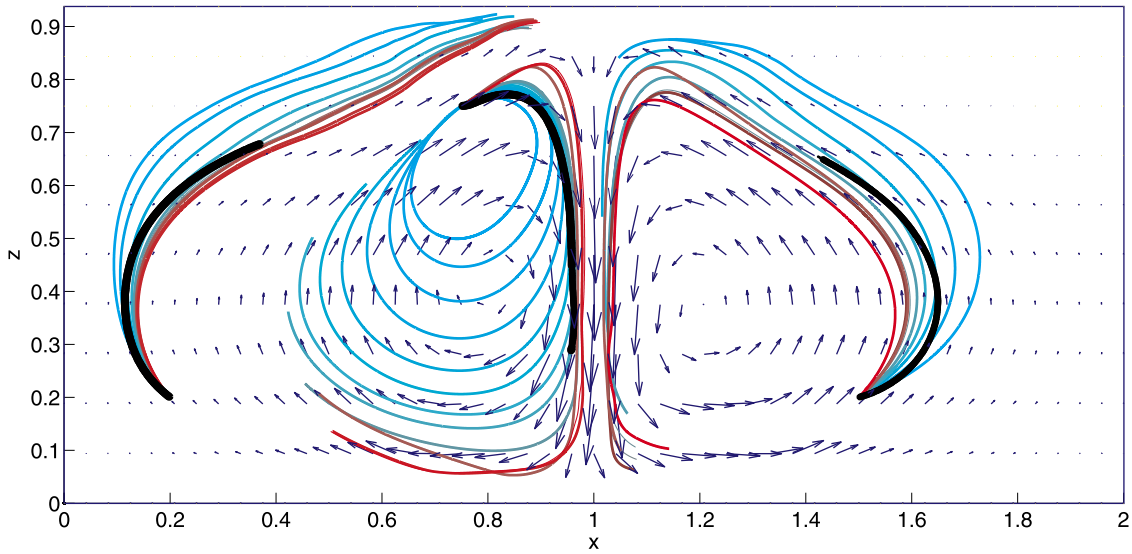

Figure 5. Changes in particle trajectories for a particle starting at the same spot and advected by the different velocity fields resulting from a sinking of a dense drip at different time steps (cyan, early steps; red, late steps). Plotted in black are the actual paths of the particles as they are advected at each time step by the instantaneous velocity field associated with that time step. The arrows sketch the velocities at a time step toward the end of the calculation.

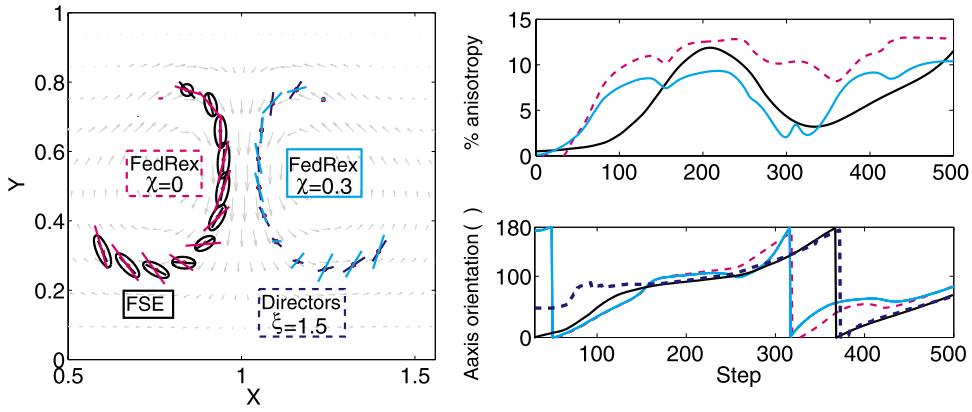

Figure 6. Results for a steady state Rayleigh-Taylor instability test. We compare the orientation of the finite strain ellipse major axis and the calculated A axis for a single advected aggregate. The predictions made by the three methods are usually aligned with the direction of the flow and, for the most part, agree with each other. (left) The grey arrows in the background reflect the velocity field. Black ellipses and lines depict the finite strain ellipses and their major axes. Cyan and pink lines show results from FedRex, for $\chi = 0$ (pink) and $\chi = 0.3$ (cyan). Blue lines show the resulting A axis orientation from advection of a set of 40 directors. (right) With line colors matching the colors in Figure 6 (left): (top) the percent of anisotropy estimated by the FedRex and FSE methods, calculated as $(Vp1 - Vp2)/(Vp1 + Vp2) \times 100$; (bottom) A axis orientation (in degrees from the horizontal) for the three methods.

[27] Figure 6 displays the evolution of olivine LPO, orientation and magnitude, calculated using FedRex (cyan, pink), Directors (blue), and the FSE (black) methods. There is usually good agreement between the predictions of three methods along the particle path, with some deviation at the beginning of the path.

[28] In Figure 7 we show the anisotropy field calculated using directors as it evolves and develops over time. The LPO is calculated by averaging over a much coarser grid than the one used in the

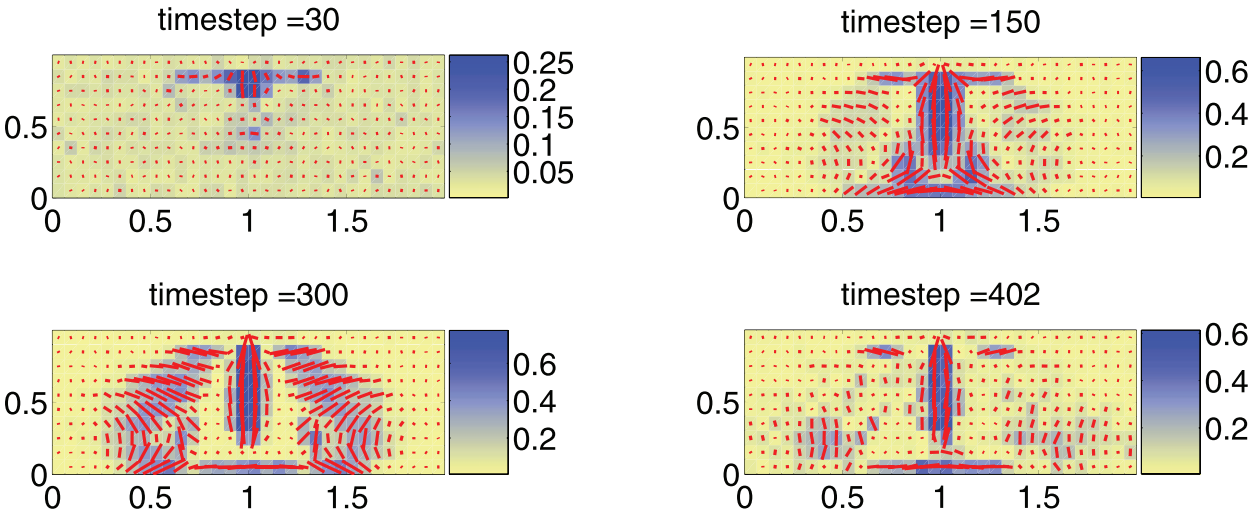

Figure 7. Time evolution of the anisotropy, calculated using the Directors method, in a model of a Rayleigh-Taylor instability driven by density layering. The background color of each panel shows the M index, a metric of the strength of the anisotropy within that block. The range of M index is zero (no LPO) to 1 (complete alignment). The red bars show the direction of the A axis as calculated by averaging the orientations of the director within the block. Note that the element resolution of the initial finite element calculation is much higher than the blocks used for the averaging presented here.

finite elements calculation of the flow field (32 × 10 blocks versus 240 × 32 elements), to make it more comparable to the wavelength of seismic waves used to study mantle anisotropy (SKS, for example). Figure 7 demonstrates how the directors method is readily capable of tracking the development of anisotropy within a region over time.

4. Discussion

4.1. Infinite Strain Axis Versus Directors

[29] A variant of the FSE technique is the calculation of the Infinite Strain Axis (ISA), defined as the orientation of the FSE after being subjected to a constant velocity gradient for infinite time [*Kaminski and Ribe*, 2002]. This technique gives a quick estimation of the anisotropy orientation, and it has been proven to approximate the prediction of the crystallographic technique of D-Rex well through most of the Earth's mantle [*Conrad et al.*, 2007]. Unlike the tracking of the FSE, the ISA at a given time and place does not depend on the path, and therefore is not influenced by the assumed initial conditions. However, this method was shown to give poor results in regions of Earth that deform more slowly, such as the more rigid lithosphere, and thus cannot be used to estimate ''frozen-in'' anisotropy [*Conrad et al.*, 2007]. Another limitation of the ISA technique is that in parts of the mantle where the velocity gradient changes rapidly along a streamline, or where the rotational component is larger than the straining component, the ISA might not be defined. Examples for such regions are places of strong downwelling or upwelling through the asthenosphere, such as active plate boundaries (subduction zones and mid-ocean ridges), as well as small-scale convection [e.g., *Montagner*, 2002; *van Hunen et al.*, 2005]. Since these regions are quite often the focus of geophysical interest, as well as the source of many of the observations of anisotropy, an alternative fabric prediction technique is required.

4.2. Computation Cost and Availability of the Methods

[30] The vast majority of the predictions of anisotropy come from mantle flow models that, in fact, assume isotropic rheology. *Lev and Hager* [2008] showed that including anisotropic viscosity and allowing for mutual feedback between the deformation, the rheology and the anisotropy, changes the flow. This kind of self-consistent modeling requires a texture prediction technique that is efficient and fast, as well as suitable for a straightforward integration with geodynamic flow calculation codes. The computational cost of each of the methods is also important when long or time-dependent calculations are considered. We analyze here the computational cost involved with the directors method and compare it with that of FedRex.

[31] Our measurements of Underworld runs (Figure S1 in the auxiliary material) indicate that approximately 30% of the program execution time is spent on the time integration of the director orientation and length parameters.[1] This percentage is almost independent of the finite element mesh size or the number of directors. The total number of directors strongly controls the overall duration of calculation, as it is the most time-consuming stage.

[32] For a single particle, the calculation of the FSE takes 4 times longer than the director. However, we find that in order to obtain a meaningful average orientation for a set of directors, at least 10 are needed if realignment is not applied, and at least 30 are needed if realignment is applied. This makes the directors method 8 times slower than the FSE method. On the other hand, the use of a large set of directors facilitates the simulation of a continuous recrystallization process. To achieve this using FSEs would require averaging a set of ellipses and would make the computational cost of the two methods comparable.

[33] The computational cost of the Directors methods is still low compared with that of FedRex, as the Directors method is both faster and requires much less memory. At every time step, we advance the orientation of each director using equation (3) and a second-order Runge-Kutta integration scheme. We compare the length of the new director and calculate the accumulated stretch, and, if needed, realign the director. This is a much simpler calculation than the calculation done in FedRex, where three vectors are rotated for each grain, and the energy of slip systems, as well as the change in the volume fraction of each grain, are calculated. Our tests reveal that Underworld's execution time-scales with the square root of the number of directors (Figure 8), while FedRex scales linearly and quite strongly with both the grid size and the number of grains per aggregate (Figure 9). To obtain the same model resolution and accuracy with both methods, one would need a very large

[1] Auxiliary materials are available in the HTML. doi:10.1029/2008GC002032.

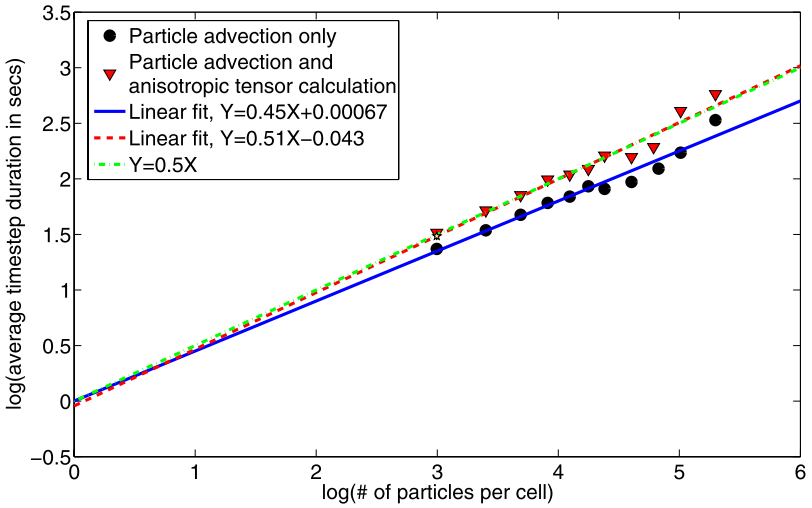

Figure 8. Underworld execution time (log) for a 2-D model of Rayleigh-Taylor instability with a 64 × 64 elements grid, as a function of the number of directors per element (log). Circles, blue line show the results for advection of isotropic particles (no tracking of orientation); triangles, red line show the results for advection of directors, including tracking of orientation and length. The green dashed line has a slope of 0.5, underlining the observation that the execution timescales as the square root of the number of particles.

number of aggregates in FedRex, which would lead to a much longer execution time. It is also interesting to note that in the current implementation of FedRex, approximately 50% of the run time is spent on the time integration phase, and over 50% of the run time is spent on calculating the Voigt average of grain orientations to obtain the complete tensor of the aggregate. The directors method uses a simpler, finite element style, averaging scheme and is thus faster in this stage as well. These differences make the directors method notably faster. Therefore, including a FedRex-like calculation in a flow code would increase its execution time significantly.

[34] In addition, the Directors method requires less memory. Because of the assumption of hexagonal symmetry, each director is represented solely by a vector and an accumulated stretch value, a total of four numbers (3-D) or three numbers (2-D). FedRex, on the other hand, keeps a nine-element matrix of cosine angles (representing the orientation of the three crystallographic axes) for each grain, as well as a vector holding the fractional grain volumes and matrices holding the derivatives of these matrices. We also find that an aggregate of less than 100 directors gives a stable solution that compares well with an aggregate of ∼1000 grains in FedRex.

[35] One important factor for the modeling community is that the Directors method is implemented in the C language and is already embedded in the advanced geodynamics codes Underworld and Gale. D-Rex and FedRex are written in Fortran, which makes the integration with geodynamics codes, commonly written in C, less straightforward. This ease of integration is valuable for applications studying the effect of the development of anisotropy on flow models through feedback

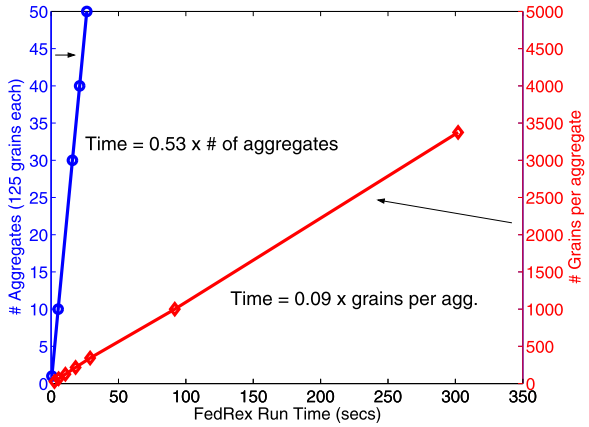

Figure 9. FedRex execution time plotted against the number of aggregates propagated through the model domain (blue, circles), and against the number of grains per aggregate (red, diamonds). The stronger dependence on the number of aggregates indicates that more time is spent on per-aggregate calculations such as Voigt averaging and propagation in space, compared to time spent on per-grain calculations. Specifically, our measurements reveal that the Voigt averaging is the time-consuming stage.

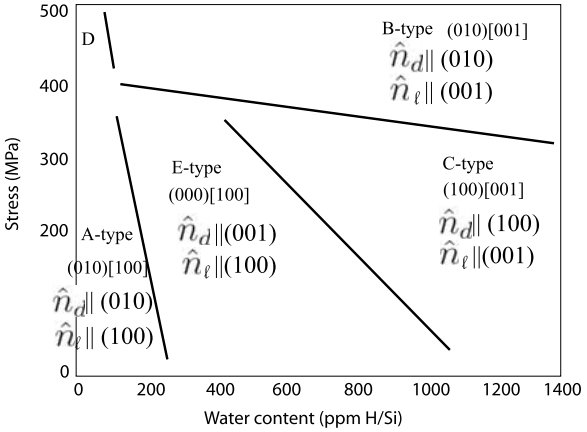

Figure 10. Types of olivine LPO as a function of water content and stress [after *Zhang et al.*, 2000]. For each type for which the dominant slip system is known, we identify the relationship between the a, b, and c axes and the directors. The $\hat{n}_d$ is the director orientation and n_ℓ is the lineation. This matching can help translate from a given orientation of directors and local model conditions (stress, water content, temperature, pressure) to predicted seismic anisotropy, keeping in mind the assumption about the relative wave speeds along the crystal axes.

between deformation and rheology [*Mühlhaus et al.*, 2004; *Lev and Hager*, 2008].

4.3. Relating Director Orientations and Olivine Seismic Anisotropy

[36] The directors, by their very definition, imply a high symmetry of the tracked aggregates with respect to deformation and viscosity. The directors define an easy glide plane, representing a dominance of one family of easy slip systems that can be written as $(010) < h0\ell >$ (with the director set as the (010) b axis). This kind of slip is common in minerals such as graphite, calcite, quartz and mica. In dry olivine, however, the dominant slip systems at relatively low stress, pressure and temperature conditions are (010)[100] and (001)[100], while the system (010)[001] is more resistant [e.g., *Zhang and Karato*, 1995; *Tommasi*, 1998]. Under different temperature, water content and stress conditions the dominant slip system of olivine changes (Figure 10). Approximating olivine rheology with the layered type of rheology implied by the basic definition used by *Mühlhaus et al.* [2004] and *Lev and Hager* [2008] means that the director orientation $\hat{n}_d$ is identified with the olivine *b* axis and that the relative strength of the olivine slip systems is only partially accounted for. Nonetheless, the generality of the directors enables us to relate the predicted mantle seismic anisotropy to the developed orientation of easy glide planes by taking into account the local P, T and water conditions. We suggest assuming that the directors define the normal to the foliation planes. To choose the lineation direction, which is inherently nonunique by the definition of the directors, we use the projection of the local direction of maximum shear (based on the velocity gradient) onto the foliation plane. Figure 1 depicts the various orientations defined above.

[37] The seismic velocities in different directions in olivine crystals depend mostly on the lattice structural density, and not on the dominant slip system. The *a* axis is considered to always be the fast propagation direction [*Babuška and Cara*, 1992]. The relationship between the seismically fast direction and the foliation/lineation system depends on which slip system is active, which, in turn, depends on the local conditions. For A-type olivine LPO, the seismically fast *a* axis is oriented parallel to the lineation, and the *b* axis is oriented normal to the foliation (thus parallel to the directors). In B-type olivine LPO, perhaps relevant to hydrated subduction zone conditions, the *b* axis is still normal to the foliation and parallel to the director, but the a axis is normal to the lineation (and the c axis is parallel to the lineation). A more general algorithm would be to track the orientation of the crystal axes, and infer the direction of the easy glide planes given the local conditions and the activity of the various slip systems they imply. The algorithm described above, however, would enable us to translate the orientation we track for the sake of rheological anisotropy to orientations relevant to crystal orientations and the seismic anisotropy quickly and cheaply, and using tested tools that already exist. To quickly deduce orientation and strength of the anisotropy represented by a set of closely spaced directors, we take an angular averaging of their directions, and calculate the M index [*Skemer et al.*, 2005], as we demonstrate in Figure 7.

[38] In section 4.2 we compared the directions of LPO axes predicted by the three methods and showed that the directors and the crystallographic code agree for all three test cases. However, the directors are only capable of representing cubic and hexagonal symmetries, while FedRex calculates the evolution of the full elastic tensor of the aggregates. It is thus important to determine how much of the anisotropy predicted by FedRex is due to hexagonal symmetry and can be reproduced

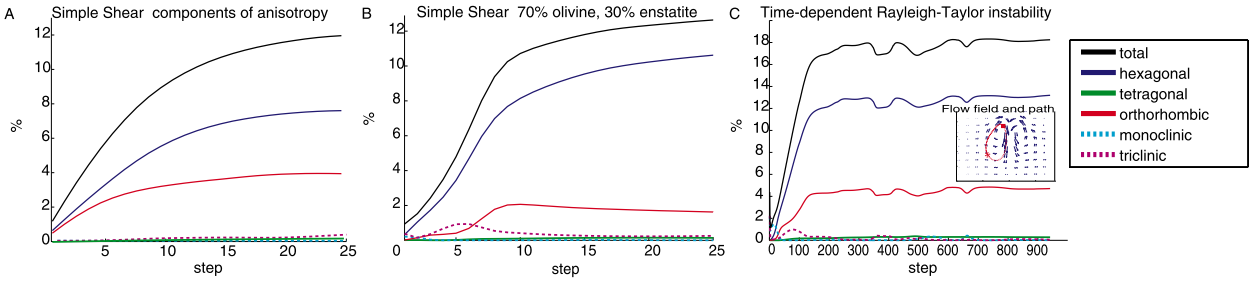

Figure 11. The proportions of the symmetry components in the total anisotropy of a deformed aggregate, as predicted by FedRex. (a) simple shear test with 100% olivine, (b) simple shear test with 70% olivine and 30% enstatite, and (c) a drip flow model with 100% olivine. In all cases, and mostly for the more realistic composition of 70% olivine, the hexagonal component makes the predominant part of the anisotropy. For the simple shear test of a 100% olivine aggregate, the orthorhombic component is also somewhat large. The inset shows the velocity field and particle path used for this calculation. The hexagonal component again is responsible for most of the anisotropy. The insets show two views of the velocity field and particle path used for this calculation. The red bars show the A axis of the propagated aggregate.

safely by the directors, and how much requires a more sophisticated treatment. We added to FedRex an implementation of the method of *Browaeys and Chevrot* [2004], in which the full elastic tensor at every step of the flow is decomposed into its different symmetry components: isotropic, hexagonal, orthorhombic, tetrahedral, monoclinic and triclinic, in decreasing order of symmetry. We first tested a simple shear case for two aggregate compositions: one made of 100% olivine and one of 70% olivine and 30% enstatite. We then propagated an olivine aggregate with initially random orientation through a Rayleigh-Taylor instability model and checked the patterns of crystallographic symmetry that develop.

[39] The results, plotted in Figure 11, show clearly that for the cases tested, the hexagonal component of the symmetry describes the lion's share of the anisotropy. (Note that although the flow is 2-D plane strain, the initial random fabric is 3-D, so the fabric retains a small component of orthorhombic symmetry.) We conclude therefore that the approximation made by using directors may be valid in most cases relevant to the mantle.

5. Summary

[40] We compare three methods for calculating fabric from a given velocity field: tracking of the finite strain ellipse, a kinematic crystallographic code, and the evolution of directors. We find that the use of finite strain ellipses can provide only limited accuracy for fabric evolution prediction, as it does not take into account the process of recrystallization. The kinematic code D-Rex, after some modification, provides a more complete method for fabric prediction, but its computational cost is significantly higher. This high computational cost, as well as its lower integrability, limits D-Rex's usefulness for large-scale geodynamical flow models. The directors provide an intermediate solution: while they inherently imply higher symmetry than the full crystal structure considered by D-Rex, as well as ignoring the physical basis of some of the more complex crystallographic processes D-Rex includes, the overall results of this method closely resemble those computed via D-Rex, at a lower computational cost. In conclusion, when computation speed is important, for example, in self-consistent geodynamic flow models that incorporate anisotropy into the model rheology, the directors method provides an appropriate approximation.

Acknowledgments

[41] We are thankful for helpful discussions with Jessica Warren, Nick Austin, Laurent Pouilloux, and Andrea Tommasi. Reviews by Eduard Kaminski and an anonymous reviewer are greatly appreciated and helped improve this manuscript. The research presented here was supported by NSF grant EAR-0409564.

References

Baba, K., A. D. Chave, R. L. Evans, G. Hirth, and R. L. Mackie (2006), Mantle dynamics beneath the East Pacific Rise at 17S: Insights from the Mantle Electromagnetic and Tomography (MELT) experiment, *J. Geophys. Res.*, *111*, B02101, doi:10.1029/2004JB003598.

Babuška, V., and M. Cara (1992), *Modern Approaches in Geophysics*, vol. 10, *Seismic Anisotropy in the Earth*, Kluwer Acad., Dordrecht, Netherlands.

Becker, T. W., J. B. Kellogg, G. Ekström, and R. J. O'Connell (2003), Comparison of azimuthal seismic anisotropy from surface waves and finite strain from global mantle-circulation models, *Geophys. J. Int.*, *155*, 696–714, doi:10.1046/j.1365-246X.2003.02085.x.

Becker, T. W., S. Chevrot, V. Schulte-Pelkum, and D. K. Blackman (2006a), Statistical properties of seismic anisotropy predicted by upper mantle geodynamic models, *J. Geophys. Res.*, *111*, B08309, doi:10.1029/2005JB004095.

Becker, T. W., V. Schulte-Pelkum, D. K. Blackman, J. B. Kellogg, and R. J. O'Connell (2006b), Mantle flow under the western United States from shear wave splitting, *Earth Planet. Sci. Lett.*, *247*, 235–251, doi:10.1016/j.epsl.2006.05.010.

Ben-Ismail, W., G. Barruol, and D. Mainprice (2001), The Kaapvaal Craton seismic anisotropy: Petrophysical analyses of upper mantle Kimberlite nodules, *Geophys. Res. Lett.*, *28*, 2497–2500.

Blackman, D. K., H.-Rudolf Wenk, and J. M. Kendall (2002), Seismic anisotropy of the upper mantle: 1. Factors that affect mineral texture and effective elastic properties, *Geochem. Geophys. Geosyst.*, *3*(9), 8601, doi:10.1029/2001GC000248.

Browaeys, J. T., and S. Chevrot (2004), Decomposition of the elastic tensor and geophysical applications, *Geophys. J. Int.*, *159*, 667–678, doi:10.1111/j.1365-246X.2004.02415.x.

Chastel, Y. B., P. R. Dawson, H.-R. Wenk, and K. Bennett (1993), Anisotropic convection with implications for the upper mantle, *J. Geophys. Res.*, *98*, 17,757–17,771.

Conrad, C. P., M. D. Behn, and P. G. Silver (2007), Global mantle flow and the development of seismic anisotropy: Differences between the oceanic and continental upper mantle, *J. Geophys. Res.*, *112*, B07317, doi:10.1029/2006JB004608.

Durham, W. B., and C. Goetze (1977), Plastic flow of oriented single crystals of olivine: 1. Mechanical data, *J. Geophys. Res.*, *82*, 5737–5754.

Fischer, K. M., and D. A. Wiens (1996), The depth distribution of mantle anisotropy beneath the Tonga subduction zone, *Earth Planet. Sci. Lett.*, *142*, 253–260.

Fouch, M. J., and S. Rondenay (2006), Seismic anisotropy beneath stable continental interiors, *Phys. Earth Planet. Inter.*, *158*, 292–320, doi:10.1016/j.pepi.2006.03.024.

Hall, C. E., K. M. Fischer, E. M. Parmentier, and D. K. Blackman (2000), The influence of plate motions on three-dimensional back arc mantle flow and shear wave splitting, *J. Geophys. Res.*, *105*, 28,009–28,033.

Jousselin, D., and D. Mainprice (1998), Melt topology and seismic anisotropy in mantle peridotites of the Oman ophiolite, *Earth Planet. Sci. Lett.*, *164*, 553–568.

Jung, H., and S. Karato (2001), Water-induced fabric transitions in olivine, *Science*, *293*, 1460–1463.

Kaminski, É., and N. M. Ribe (2001), A kinematic model for recrystallization and texture development in olivine polycrystals, *Earth Planet. Sci. Lett.*, *189*, 253–267.

Kaminski, É., and N. M. Ribe (2002), Timescales for the evolution of seismic anisotropy in mantle flow, *Geochem. Geophys. Geosyst.*, *3*(8), 1051, doi:10.1029/2001GC000222.

Kaminski, É., N. M. Ribe, and J. T. Browaeys (2004), D-Rex, a program for calculation of seismic anisotropy due to crystal lattice preferred orientation in the convective upper mantle, *Geophys. J. Int.*, *158*, 744–752.

Karato, S. (1988), The role of recrystallization in the preferred orientation of olivine, *Phys. Earth Planet. Inter.*, *51*, 107–122.

Lev, E., and B. H. Hager (2008), Rayleigh-Taylor in stabilities with anisotropic lithospheric viscosity, *Geophys. J. Int.*, *173*(3), 806–814, doi:10.1111/j.1365-246X.2008.03731.x.

Long, M. D., B. H. Hager, M. V. de Hoop, and R. D. van der Hilst (2007), Two-dimensional modelling of subduction zone anisotropy with application to southwestern Japan, *Geophys. J. Int.*, *170*, 839–856, doi:10.1111/j.1365-246X.2007.03464.x.

Malvern, L. E. (1969), *Introduction to the Mechanics of a Continous Media*, Prentice-Hall, Englewood Cliffs, N. J.

Marquart, G., H. Schmeling, and O. Èadek (2007), Dynamic models for mantle flow and seismic anisotropy in the North Atlantic region and comparison with observations, *Geochem. Geophys. Geosyst.*, *8*, Q02008, doi:10.1029/2006GC001359.

Maupin, V., E. J. Garnero, T. Lay, and M. J. Fouch (2005), Azimuthal anisotropy in the D″ layer beneath the Caribbean, *J. Geophys. Res.*, *110*, B08301, doi:10.1029/2004JB003506.

McKenzie, D. (1979), Finite deformation during fluid flow, *Geophys. J. Int.*, *58*(3), 689–715, doi:10.1111/j.1365-246X.1979.tb04803.x.

Mehl, L., B. R. Hacker, G. Hirth, and P. B. Kelemen (2003), Arc-parallel flow within the mantle wedge: Evidence from the accreted Talkeetna arc, south central Alaska, *J. Geophys. Res.*, *108*(B8), 2375, doi:10.1029/2002JB002233.

Montagner, J. (1998), Where can seismic anisotropy be detected in the Earth's mantle? in boundary layers, *Pure Appl. Geophys.*, *151*, 223–256.

Montagner, J.-P. (2002), Upper mantle low anisotropy channels below the Pacific Plate, *Earth Planet. Sci. Lett.*, *202*, 263–274.

Moresi, L., F. Dufour, and H.-B. Mühlhaus (2003), A Lagrangian integration point finite element method for large deformation modeling of viscoelastic geomaterials, *J. Comput. Phys.*, *184*, 476–497.

Mühlhaus, H.-B., L. Moresi, and M. Cada (2004), Emergent anisotropy and flow alignment in viscous rock, *Pure Appl. Geophys.*, *161*, 2451–2463, doi:10.1007/s00024-004-2575-5.

Pouilloux, L., E. Kaminski, and S. Labrosse (2007), Anisotropic rheology of a cubic medium and the implications for geologic materials, *Geophys. J. Int.*, *170*, 876–885, doi:10.1111/j.1365-246X.2007.03461.x.

Ribe, N. M. (1992), On the relation between seismic anisotropy and finite strain, *J. Geophys. Res.*, *97*, 8737–8747.

Savage, M. K. (1999), Seismic anisotropy and mantle deformation: What have we learned from shear wave splitting?, *Rev. Geophys.*, *37*, 65–106.

Simpson, F. (2002), Intensity and direction of lattice-preferred orientation of olivine: Are electrical and seismic anisotropies of the Australian mantle reconcilable?, *Earth Planet. Sci. Lett.*, *203*, 535–547.

Skemer, P., I. Katayama, Z. Jiang, and S. I. Karato (2005), The misorientation index: Development of a new method for calculating the strength of lattice-preferred orientation, *Tectonophysics*, *411*, 157–167.

Tommasi, A. (1998), Forward modeling of the development of seismic anisotropy in the upper mantle, *Earth Planet. Sci. Lett.*, *160*, 1–13.

Tommasi, A., D. Mainprice, G. Canova, and Y. Chastel (2000), Viscoplastic self-consistent and equilibrium-based modeling of olivine lattice preferred orientations: Implications for the upper mantle seismic anisotropy, *J. Geophys. Res.*, *105*, 7893–7908.

van Hunen, J., S. Zhong, N. M. Shapiro, and M. H. Ritzwoller (2005), New evidence for dislocation creep from 3-D geodynamic modeling of the Pacific upper mantle structure, *Earth Planet. Sci. Lett.*, *238*, 146–155.

Weiss, T., S. Siegesmund, W. Rabbel, T. Bohlen, and M. Pohl (1999), Seismic velocities and anisotropy of the lower continental crust: A review, *Pure Appl. Geophys.*, *156*, 97–122.

Wenk, H.-R., S. Speziale, A. K. McNamara, and E. J. Garnero (2006), Modeling lower mantle anisotropy development in a subducting slab, *Earth Planet. Sci.Lett.*, *245*, 302–314, doi:10.1016/j.epsl.2006.02.028.

Zhang, Z., and S. I. Karato (1995), Lattice prefered orientation in olivine aggregates deformed in simple shear, *Nature*, *375*, 774–777.

Zhang, Z., S. I. Karato, U. H. Gerald, and Y. Zhou (2000), Simple shear deformation of olivine aggregates, *Tectonophysics*, *316*, 133–152.